HHS Public Access

Author manuscript

Mol Pharm. Author manuscript; available in PMC 2020 July 01.

Published in final edited form as:

Mol Pharm. 2019 July 01; 16(7): 2872–2883. doi:10.1021/acs.molpharmaceut.8b01343.

Alendronate-modified polymeric micelles for the treatment of breast cancer bone metastasis

Tong Liu[1], **Svetlana Romanova**[1], **Shuo Wang**[2], **Megan A. Hyun**[2], **Chi Zhang**[2], **Samuel M. Cohen**[3], **Rakesh K. Singh**[3], and **Tatiana K. Bronich**[*,1]

[1]University of Nebraska Medical Center, Department of Pharmaceutical Sciences, 983135 Nebraska Medical Center, Omaha, NE 68198-3135, USA

[2]University of Nebraska Medical Center, Department of Radiation Oncology, Fred & Pamela Buffett Cancer Center, 983135 Nebraska Medical Center, Omaha, NE 68198-3135, USA

[3]University of Nebraska Medical Center, Department of Pathology and Microbiology, 983135 Nebraska Medical Center, Omaha, NE 68198-3135, USA

Abstract

Although the prognosis of patients with breast cancer continues to improve, breast cancer metastasis to bones remain high in incidence and challenging to manage. Here we report the development of bone-homing alendronate (ALN)-anchored biodegradable polymeric micelles for the targeted treatment of metastatic cancer to bone. These micelles exhibited bone protective capacity including the recruitment, differentiation and resorption activity of the osteoclasts. Encapsulation of docetaxel (DTX), the first-line chemotherapeutic for treatment of metastatic breast cancer, in ALN-modified micelles results in a sustained release, enhanced cytotoxicity and improved pharmacokinetics. In the syngeneic animal model of late-stage disseminated breast cancer bone metastasis, the treatment with targeted DTX-loaded micelles attenuated the tumorigenesis and significantly improved animal lifespan compared to the conventional surfactant-based formulation (free DTX). These findings indicate potential applications of the osteotropic nanomedicines for bone metastasis treatment.

Keywords

Nanomedicine; Bone Targeting; Polymeric Micelles; Breast Cancer Bone Metastasis

[*]Corresponding author: tbronich@unmc.edu; Tele: 402-559-9351; Fax: 402-559-9365.

Supporting information. 1H-NMR spectra of synthesized block copolymers (ALK-PEG-PBGlu10 and ALK-PEG-PBGlu10-PPhA10); polymer characteristics determined by 1H-NMR and GPC; GPC traces of ALK-PEG-NH2, ALK-PEG-PBGlu10 and ALK-PEG-PBGlu10-PPhA10 (DMF + 10 mM LiCl; 40 °C); CMC for the polymers ALK-PEG-PGlu10-PPhA10 and (B) ALN-PEG-PGlu10-PPhA10; binding of the micelles to the bone mineral HA in DI water (in the presence of 3.4 mM CaCl2); PK parameters of DTX in plasma in tumor-free nude mice; in vitro toxicity (MTT assay) of empty ALN-m and ALK-m (4T1 cancer breast cells; 36 h at 37 °C); histogram of fluorescence signal and median fluorescence intensity (MFI) of Cy5-labeled ALN-m/DTX and ALK-m/DTX (4T1 cells; 5 × 105; 2 h; 37 °C); BLI images and quantification of bone metastasis burden in individual mice (at day 0 and day 6) treated with different formulations; histopathological analysis of representative kidney, liver, and spleen of mice received different treatments; quantification of bone metastasis burden in individual mice treated with radiotherapy alone or combination of ALN-m/DTX and radiotherapy. This material is available free of charge via the Internet at http://pubs.acs.org.

INTRODUCTION

Tumor metastases remain the primary cause of cancer-related mortality. Bone has been widely recognized not only as one of the frequent destinations of metastatic spread of multiple solid tumors, but also as an organ that can offer a favorable microenvironment for cancer cell survival and further growth or dormancy of metastases. The complex mechanism of bone metastasis involves a coordinating interplay of bone-homing cancer cells, osteoclasts, osteoblasts and the immune cells in the bone marrow[1]. Tumor cells produce factors which stimulate osteoclastic bone resorption and negatively affect osteoblasts. The consequent release of bone-derived growth factors that act on cancer cells, promotes a more aggressive tumor phenotype and potentiate cancer spread and bone destruction. Moreover, physical properties of bone, such as acidic pH, a high extracellular calcium concentration and hypoxia, also support tumor growth. In patients with breast cancer, the skeleton is the most frequent site for metastases. It is estimated that up to 75% of late-stage breast cancer patients will eventually develop bone metastases[2]. These lesions lead to various skeletal complications, including osteolysis, hypercalcemia, bone pain, pathologic fractures, and spinal cord and nerve compression syndromes[3]. These complications increase morbidity and diminish the quality of life in such patients as well as often account for the poor prognosis[4]. During the past few decades, the advances in early diagnosis and development of more effective treatment strategies led to significant reduction in mortality from primary breast cancer. However, the current therapeutic modalities for advanced metastatic breast cancer patients remain palliative. Radiation therapy remains to be a gold standard for palliative care of bone metastases and suppression of local disease. Osteoclast inhibitors, bisphosphonates (zoledronic acid, pamidronate) and denosumab, an antibody targeting RANKL, are commonly prescribed therapeutics for management the progression of the established disease and reducing the risk of occurrence of skeletal-related events. However, the impact of these agents on survival outcomes was seen in only a small population of patients[5,6]. Another challenge in the treatment of bone metastatic disease is effective delivery of therapeutics to the tumor sites due to poor penetration of most drugs in the bone tissue. Moreover, these agents also affect non-cancerous cells within the bone microenvironment, impeding bone healing processes and potentially leading to some adverse events. Thus, despite significant advances in the care of these patients there is a need for more effective treatment options to prolong the survival of patients with metastatic bone diseases.

During the last decades, substantial attempts have been made in targeting bone metastases using drug delivery systems such as polymer-drug conjugates, liposomes, polymeric nanoparticles and micelles. These systems aim to improve the biodistribution and target site accumulation of drugs thus reducing side effects. To further enhance targeting of nanoparticles to bone lesions, the bone-binding moieties, such as bisphosphonates, were utilized as targeting ligands due to their affinity to the mineral compartment in bone tissue[7,8]. Indeed, hydroxyapatite is exposed as bone metastases progress offering a target for bisphosphonate binding. In line with this, detection of metastatic involvement of the skeleton using ^{99m}Tc - radiolabeled bisphosphonates has been in clinical practice for many years[9]. A number of *in vitro* and *in vivo* studies substantiated preferential and efficient accumulation of bone-targeted drug carriers within the bone lesions. Interestingly, despite demonstrated

improved drug efficacy, reduced toxicity and delay of disease progression in mouse models, no significant survival improvement between targeted and non-targeted nanocarriers has been reported[10–17]. Nonetheless, combining the benefits of drug delivery systems with bisphosphonate bone targeting to influence the tumor cells and their microenvironment may further improve the capabilities of drug delivery to eliminate or ameliorate bone metastases.

Herein, we engineered bone-homing polypeptide-based polymeric micelles carrying the chemotherapeutic docetaxel for the treatment of breast cancer bone metastases. To achieve this, an amphiphilic triblock copolymer composed of polyethylene glycol, polyglutamic acid and polyphenylalanine (PEG-PGlu-PPhA) was functionalized with a bisphosphonate, alendronate (ALN). The phenylalanine moieties facilitate self-association of block copolymers and formation of micelles and are essential for solubilization of hydrophobic compounds. Using an immunocompetent mouse model of breast cancer dissemination to the bone, this study demonstrates that targeted micelle-based therapy significantly attenuated tumor burden and extended animal survival, proving the effectiveness of this targeting approach for the delivery of chemotherapeutics to the bone.

MATERIALS AND METHODS

MATERIALS

α-Amino-ω-ALK-poly(ethylene glycol) (ALK-PEG-NH_2, M_W = 5,000 g mol^{-1}, Đ = 1.02) was purchased from JenKem Technology USA Inc. L-glutamic acid γ-benzyl ester (BGlu), L-phenylalanine (PhA), 1-(3-dimethylaminopropyl)-3-ethylcarbodiimide hydrochloride (EDC), N-hydroxysuccinimide (NHS), tris(3-hydroxypropyltriazolylmethyl)amine (THPTA), hydroxyapatite (HA, powder, 10μm, ≥100 m^2/g), ethylenediaminetetraacetic acid (EDTA), 3-bromopropionic acid, sodium ascorbate, copper (II) sulfate pentahydrate, Phosphate Colorimetric Kit (MAK030), Acid phosphatase Leukocyte (TRAP) Kit, and other chemicals were purchased from Sigma-Aldrich. Receptor activator of nuclear factor kappa-B ligand (RANKL) was obtained from R&D System. Docetaxel (DTX) was purchased from Selleck Chemicals LLC. Alendronate sodium trihydrate (ALN) was purchased from Alfa Aesar. CF488A amine was obtained from Biotium. Fetal bovine serum (FBS), RPMI 1640 medium, DMEM medium, penicillin/streptomycin, and other chemicals were purchased from Invitrogen. XenoLight D-Luciferin - K^+ Salt Bioluminescent Substrate was purchased from PerkinElmer.

METHODS

Synthesis of ALK-PEG-$PGlu_{10}$-$PPhA_{10}$ block copolymers.—Synthesis of the monomers, BGlu-NCA (γ-benzyl L-glutamate-N- carboxyanhydride) and PhA-NCA (L-phenylalanine -N- carboxyanhydride), and polymerizations were carried out as described previously[18]. Under inert and dry conditions, BGlu-NCA (79.6 mg, 0.302 mmol) dissolved in 5 mL of DMF was added to ALK-PEG-NH_2 (150 mg, 0.03 mmol) dissolved in 10 mL of anhydrous DMF. The reaction was carried out for 72 h at 40°C. The degree of polymerization of BGlu block was determined by ^{1}H NMR by comparing the peak intensities of the methylene protons of γ-benzyl groups and PEG (400 MHz, DMSO-d_6, δ ppm: 5.14 (m, 2H, -$CH_2C_6H_5$); 3.52 (s, 4H, -OCH_2CH_2-)). After the completion of the

reaction, PhA-NCA (145 mg, 0.26 mmol), previously dissolved in 5 mL of anhydrous 1,4-dioxane, was added and let to react for 120 h. The final product was purified by repeated precipitation from DMF into diethyl ether. The protecting benzyl groups were removed using 0.5 N NaOH. and the crude product was dialyzed against distilled water for 48 h (MWCO 2 kDa), filtered (0.8 μm filter) and lyophilized.

Synthesis of azido-ALN.—3-azidopropionic acid was synthesized as previously described[19]. To 3-azidopropionic acid (40.8 mg, 0.3 mmol) dissolved in 1 mL of anhydrous CH_2Cl_2, EDC (66 mg, 0.3 mmol) and NHS (48.6 mg, 0.4 mmol) were added and the reaction mixture was stirred for 6 h at r.t. followed by removal of the solvent under reduced pressure. The NHS activated 3-azidopropionic acid (14.6 mg) dissolved in 0.2 mL of acetonitrile/water mixture (1:4 v/v) was then added dropwise to ALN (12.3 mg, 0.04 mmol) solution in 0.5 mL of water while adjusting pH to 8.0 after each drop. The reaction was carried out overnight at r.t., then product was isolated by repeated precipitation in ethanol and dried. The structure was confirmed by ^{1}H NMR.

Synthesis of ALN-PEG-PGlu-PPhA.—The azide-ALN (6.64 mg, 0.02 mmol) and ALK-PEG-$PGlu_{10}$-$PPhA_{10}$ (13.4 mg, 0.002 mmol) were dissolved in 10 mL of water and methanol mixture (1:1 v/v). Copper (II) sulfate pentahydrate (0.5 mg, 0.002 mmol), THPTA (1.06 mg, 0.002 mmol) and ascorbic acid (3.52 mg, 0.02 mmol) were then added and reaction mixture was stirred for two days at r.t under argon atmosphere. Then, EDTA (6.7 mg, 0.02 mmol) was added to the solution followed by dialysis against deionized water (MWCO 2 kDa) for 48 h. The dialyzed solution was then acidified and lyophilized to produce ALN-PEG-PGlu-PPhA. The residual copper content after purification was 0.7 ppm as determined by inductively coupled plasma mass spectrometry.

Polymer characterization.—The ^{1}H NMR spectra were recorded in DMSO-d_6 on a Bruker 400 MHz spectrometer. Gel permeation chromatography (GPC) was performed on Shimadzu liquid chromatography system equipped with TSK-GEL® column ($G4000H_{HR}$) using DMF/LiBr (10 mmol) as mobile phase. The column was kept at 40°C and flow rate was 0.6 mL/min. Standard curve was generated using poly(ethylene glycol) standards (molecular weight range of 282 – 34,890,Agilent Technologies, USA). Critical micelle concentrations of ALK-PEG-PGlu-PPhA and ALN-PEG-PGlu-PPhA copolymers were determined using pyrene assay[20]. The ALN conjugation efficiency was determined by phosphate assay as previously reported[21]. Briefly, 20 μL of ALN-PEG-PGlu-PPhA solution (5 mg/mL) was mixed with 20 μL of H_2O_2 and 120 μL H_2SO_4 in the ampule and the mixture was heated for 15 min at 200 °C. 1.38 mL of $Na_2S_2O_5$ (3 mg/mL) was added to the ampule and samples were incubated at 100 °C for another 15 min. Finally, the sample was filtered through a 0.2 μm filter and 200 μL of the solution were collected into a 96 well plate. A series of standards was prepared in the same plate according to the manufacture's instruction ranging from 2.5 to 100 μM. Finally, 30 μL of the phosphorus reagent was added to each well, incubated with mild shaking overnight at r.t. followed by measuring the absorbance at 650 nm.

Polymeric micelles preparation and characterization.—Micelles were prepared using nanoprecipitation method. Briefly, the polymers without or with DTX were dissolved in a minimal amount of 80% ethanol (e.g. 1 mg polymer, 0.25 mg DTX in 50 μL ethanol, polymer/drug molar ratio 0.4 : 1), and dispersed into an excessive amount of ice-cold water or PBS solution (water: ethanol = 20: 1 v/v). The solutions were stirred for an additional 5 min and ethanol was evaporated under vacuum. The unbound drug was removed by centrifugation (1000 g, 5 min). Quantification of DTX in micellar formulations was performed by high-performance liquid chromatography (HPLC) HPLC analysis on Agilent 1200 HPLC system equipped with Nucleosil C18 column (250 mm × 4.6 mm) using mobile phase comprised of acetonitrile/water mixture (55/45, v/v) at a flow rate of 1 mL/min Detection was performed at 227nm. The loading capacity (LC) was expressed as $\text{LC}\ (\%) = \frac{W_{DTX}}{W_{DTX} + W_{polymer}} \times 100\%$, where w_{DTX} and $w_{polymer}$ are the weight amount of solubilized drug and polymer excipients in solution. The hydrodynamic diameters (D_{eff}), polydispersity index (PDI) and ζ-potential of the drug-loaded micelles were evaluated by dynamic light scattering (DLS) using Nano ZS Zetasizer (Malvern Instruments, UK) at 25°C. Results are presented as means ± SD (n = 3).

Drug release studies.—The release profiles of DTX were measured in PBS (pH 7.4) or 70% FBS in PBS at 37 °C. Briefly, 1 mL of micelle formulation in PBS (approximately 0.1 mg/mL of DTX) was loaded into a Slide-A-Lyzer G2 dialysis tube (MWCO 3.5 kDa) and suspended in 45 mL PBS solution. At predetermined time points, samples of 100 μL were collected from the dialysis device and DTX concentrations were quantified by HPLC using the same conditions reported above.

HA binding assay.—To investigate the biomineral-binding ability of ALN-functionalized micelles, CF-488 labeled copolymers were synthesized by EDC coupling (at a molar ratio of [COOH]/[dye] = 10] and purified by dialysis to remove the uncoupled dye. The CF-488 labeled micelle solution in PBS (1.1 mg/mL, 1.5 mL) were incubated with HA powder (10 mg) for 4 hours at r.t. upon gentle shaking. HA was removed by centrifugation (2200 g, for 1 min) and the fluorescence intensity of the supernatant ($I_{supernatant}$) was recorded at 515 nm (λ_{ex}=490 nm) and compared with the initial micelle solution (I_o). The relative binding affinity was calculated as $\left(1 - \frac{I_{supernatant}}{I_o}\right) \times 100\%$. CF-488-labeled ALK-m were used as controls. The binding test was performed in triplicate.

Cell culture and cytotoxicity studies.—The murine 4T1 mammary adenocarcinoma cell line was obtained from American Type Culture Collection (ATCC). Cells were maintained in RPMI 1640 supplemented with 10% FBS, and 100 U/mL streptomycin/penicillin at 37 °C, 5% CO_2. Cells (3500 cells per well) were seeded in the 96-well plates, cultured for 12 h and then exposed to free DTX (formulated as 10 mg DTX, 80 mg Tween 80, 648 mg PEG300, 275.9 mg ethanol 96%, 4 mg citric acid) and DTX-loaded micelles at serial concentrations for 36 h at 37 °C. The cell viability was be evaluated by standard MTT assay[22] and the IC_{50} values were calculated using GraphPad Prism software. To confirm the anticancer activity, cells were seeded in 24-well plates pre-coated with Matrigel (95 cells/

cm^2) for clonogenic assay. Cells were treated with free DTX or DTX-loaded micelles (0.1 μg/mL on DTX basis) for 36 h and allowed to recover in fresh medium for another 72 h. Colonies were washed, stained with crystal violet and counted. The surviving fraction (SF) was calculated as:

$$SF = \frac{No.\ of\ colonies\ at\ the\ end\ point\ of\ the\ study}{No.\ of\ seeded\ cells \times PE}$$

where plating efficiency (PE) is calculated as:

$$PE = \frac{No.\ of\ colonies\ after\ seeding}{No.\ of\ seeded\ cells}$$

Inhibition of osteoclastogenesis and osteoclasts absorptive activity.—The Raw264.7 monocyte/macrophage-like cells were obtained from ATCC (TIB-71) and maintained in DMEM supplemented with 10% FBS and 1% penicillin/streptomycin at 37°C. Cells were collected after reaching about 75% confluency, seeded on 48-well plates (1.25×10^4 cells/well) and supplemented with RANKL at the final concentration of 50 μg/mL. After attachment, cells were exposed to various concentrations of empty ALN-decorated micelles or non-decorated micelles (0–100 μM on ALN basis) for one week. The culture medium containing RANKL and corresponding treatment were exchanged every three days. At the end cells were fixed in 10% buffered formaldehyde and stained with TRAP. The stain-positive cells (osteoclasts) in each well were numerated to calcculatre IC_{50}. The bone resorption activity of osteoclasts derived from Raw264.7 cells was evaluated in 24-well Osteo Surface plates. Raw264.7 cells were continuously cultured with RANKL (50 μg/mL) in the presence or absence of ALN-decorated micelles or non-decorated micelles at two different concentrations (0.81 μM or 9 μM on ALN basis) for 7 days. In another setting, Raw264.7 cells cultured in the presence of RANKL for 4 days were exposed to the micelles for another 3 days. On day 8, cells were bleached and the area/numbers of the pits (resulting from the absorption activity of osteoclasts) appeared on the plate surface were quantified by using Image Pro software.

Macrophage migration assay.—Transwell permeable supports with 0.8 μm pore membranes were used for cell migration assay. Conditioned medium (CM) was collected from 4T1 culture following 12 h of incubation in serum-free DMEM at 37°C and used as the chemoattractant. 4T1 cells were plated on 24-well plates (10,000 cells per well) and cultured in serum-free DMEM for 12 h followed by replacement with CM and incubation for an additional 8 h. Raw264.7 cells (1,000 per insert) were allowed to attach to the top inserts and then were placed into the wells. The macrophages were allowed to migrate to the bottom of the top chamber for 24 hours in the presence of 4T1 cells and CM in the bottom chamber. Where indicated, ALN-decorated or non-decorated micelles were present in both top and bottom chambers throughout the assay. The wells without 4T1 cells and chemoattractant were used as negative controls. The cells on the upper side of the membrane that dis not migrate were removed and the migrated cells attached to the bottom side of the membrane were fixed in 10% formalin/PBS, stained with 0.25% crystal violet solution. and counted

with an inverted microscope using a 20× objective. Data presented as the average of five random spots for each well (n = 3).

Pharmacokinetics studies in mice.—All animal work was performed based on the protocols approved by the University of Nebraska Medical Center Institutional Animal Care and Use Committee. Pharmacokinetics of DTX and DTX-loaded micelles were determined in 8-weeks of age female Balb/C mice (Charles River Laboratories). The 18 mice were randomly divided into three treatment groups of 6 mice and given either DTX (in Tween 80/ethanol/PEG300) or DTX-loaded ALN-micelles or DTX-loaded non-decorated micelles by tail vein injection at an equivalent dose of 10 mg DTX/kg. At various time points, blood samples (100–150 μL) were collected from a submandibular vein into heparinized tubes and centrifuged at 10,000 g for 3 min. DTX was extracted from plasma samples (10 μL) using excess (40 μL) of ice-cold acetonitrile. All samples were sonicated for 1 min, centrifuged at 10,000 g for 3 min and collected clear supernatants were analyzed on LC-MS/MS system equipped with a Nucleosil C18 column (250 mm × 4.6 mm) using mobile phase of 80% acetonitrile at flow rate of 0.5 mL/min. Paclitaxel (625 ng/mL) was used as an internal standard. Calibration curves were generated by spiking plasma samples from control animals with DTX at concentration of 5–2000 ng/mL. An LC-MS/MS system equipped with triple quadrupole (QTRAP® 6500, Sciex) coupled to HPLC system (Nexera × 2, Shimadzu) was used in multiple reaction monitoring (MRM) mode as follows; m/z 853.995/876.25 → 286/308.25 for paclitaxel and 808.08/830.26 → 527/549.24 for DTX.

Evaluation of therapeutic efficacy.—To establish the animal model of breast cancer bone metastases, 1×10^4 4T1/Luc cells, constitutively expressing firefly luciferase, were suspended in 50 μL of sterile PBS and injected into the left cardiac ventricle[23] of female Balb/C mice (6-week of age) under isoflurane anesthesia. Disease progression and dissemination to the bone were followed by noninvasive bioluminescence imaging (BLI) using the IVIS Imaging System (Xenogen). Total photon flux (photons/sec) was measured from regions of interest (ROI) over the whole mouse body. On day 12 post-intracardiac injection, mice were randomized in 4 treatment groups (n = 8) and treated with saline (control group), DTX (in Tween 80/ethanol/PEG300), DTX-loaded ALN-decorated micelles and DTX-loaded non-decorated micelles at dose of 10 mg DTX/kg. Treatments were administered daily for three consecutive days via tail vein injections. At 48 h after the last treatment, 3 mice per each treatment group were euthanized, tissues (liver, spleen, kidney, bones) were collected and fixed in 10% buffered formalin. Bones were decalcified using Regular Cal Immuno (BBC Biochemical). After fixation, specimens were embedded in paraffin, then 5 micron thick sections were cut and stained with hematoxylin and eosin. The slides were evaluated with the pathologist blinded as to which group was being e valuated. The rest of the animals were sacrificed at low body condition scoring or signs of paralysis. We also used two additional groups of animals to elucidate the efficacy of targeted treatment of bone metastases in combination with radiotherapy. Metastatic-bearing mice (n = 6) received 3 i.v. injections on the daily basis of either saline or DTX-loaded ALN-decorated micelles (10 mg/kg on DTX basis). 24 h following the last dose of micelles or vehicle mice were irradiated using a medical linear accelerator, Siemens Priums® (S/N: M3068, Siemens

Healthineers, Erlangen, Germany), at a dose rate of 3 Gy/min with the total effective dose of 5 Gy.

RESULTS AND DISCUSSION

Synthesis of alendronate-conjugated polymers.

The synthesis of the parent ALK-PEG-$PGlu_{10}$-$PPhA_{10}$ copolymer and the modification of the distal end of the PEG block with ALN moieties using azide-alkyne “click” chemistry are shown in Scheme 1. The unreacted small molecules were removed by dialysis against deionized water (MWCO 2 kDa). The chemical composition, molecular mass and polydispersity of synthesized copolymers were determined by ^{1}H NMR and GPC analyses (Supporting information, Fig. S1 and S2, Table S1). The ALN conjugation efficiency was determined using a phosphate assay and was ~75%. We have previously demonstrated that the incorporation of hydrophobic PhA units into triblock copolymers confer amphiphilic properties and facilitates self-association of block copolymers in an aqueous medium[18]. An association behavior of PEG-PGlu-PPhA copolymers was confirmed using pyrene fluorescence assay (Figure S3). ALK-PEG- PGlu-PPhA exhibited low (0.05 μM) critical micelle concentration (CMC). The onset of aggregation of functionalized ALN-PEG-PGlu-PPhA chains was shifted to higher concentrations with determined CMC value of 1 μM. The observed increased CMC value is consistent with the presence of distal charged ALN groups on the polymer chains that are leading to increased repulsion between the copolymer chains upon the formation of micellar aggregates. This CMC value is still extremely low and comparable with those reported for PEG-poly(lactide) micelles (0.5–5 μM)[24,25], suggesting that micelles formed by ALN-PEG-PGlu-PPhA copolymers might exhibit good stability. As was previously demonstrated, the integration of aromatic units in the polymer chains forming the cores of the micelles can substantially improve the stability, taxane loading and retention in polymeric micelles[26]. Therefore, we believe that PhA-based cores of the micelles may provide a proper environment for the DTX loading.

Preparation of docetaxel-loaded polymeric micelles and characterization of their physicochemical properties.

DTX, a microtubule-stabilizing taxane, is used in clinic for the treatment of metastatic breast cancer[27,28]. Along with its potent anticancer activity, DTX also exhibits serious dose-limiting toxicities partly due to the formulation excipients. Polyoxylated surfactant, polysorbate 80, is utilized in Taxotere, a commercial formulation of DTX, and has been connected to observed nonallergic anaphylaxis, hypersensitivity reactions, and injection- and infusion-site adverse events[29]. Based on these considerations, we selected DTX as the model chemotherapeutic agent for solubilization into polymeric micelles. The micelle formation and drug loading were accomplished in one single step using a nanoprecipitation method. We obtained stable dispersions of DTX-loaded micelles with a loading capacity of 22.4% as was determined by HPLC and it was associated with high loading efficiency (about 97%). ALN-decorated micelles with varying ALN density were prepared by co-assembly of ALK-PEG-PGlu-PPhA and ALN-PEG- PGlu-PPhA copolymers at various molar ratios. In this way, we prepared alendronate-decorated micelles with the various proportion of ALN moieties ranging from 3.8 mol% to 75 mol%. Micelles prepared from ALK-only copolymers

(ALK-m) were used as a non-targeted control for comparison. Of note, the modification with ALN ligand practically did not change the size of the micelles: the average hydrodynamic diameters (D_{eff}) of the ALN-only micelles (ALN-m) and ALK-m in DI water at neutral pH were about 70 and 67 nm, respectively, as measured by DLS. The DTX-loaded micelles (further denoted as ALN-m/DTX or ALK-m/DTX) had a greater size (82–84 nm) than that of empty micelles and exhibited uniform size distribution (PDI < 0.2) (Table 1). Both types of micelles displayed net negative charge which can be explained by the presence and ionization of glutamic acid residues in the shell of the micelles. As expected, the ζ-potential of the ALN-m/DTX was further decreased to −32 ± 2 mV compared to −17.0 ± 1 mV for the unmodified ALK-m/DTX (Table 1), which is indicative of the existence of additional negatively charged ALN moieties on the surface of ALN-m. One of the common metabolic complications of bone metastasized breast cancer is hypercalcemia. It is characterized by elevated serum calcium level (about 3 – 3.5 mM for moderate cases) and indicates poor prognosis[30]. Therefore, we next examine how the presence of calcium ions may affect the characteristics of DTX-loaded micelle. When ALN-m/DTX were incubated in DI water in the presence of 3.4 mM Ca^{2+}, their size substantially decreased to ca. 57 nm and ζ-potential increased (Table 1). Likewise, a decrease in size and the net negative charge was observed for ALK-m/DTX, however, in the less pronounced manner. This behavior is consistent with effective chelation of calcium ions by bisphosphonate groups as well as partial neutralization of carboxylate groups of PGlu chains leading to decrease of net charge, reduced repulsions between the polymer chains in the shell of the micelles and collapse of the micelle. Similarly, the size of DTX-loaded micelles was also affected by the ionic strength: micelles prepared in PBS were substantially smaller compared to those in DI water (Table 1) due to the masking of the electrostatic repulsions in the shell of the micelles by the electrolyte (0.15 M NaCl). Interestingly, the addition of calcium ions to dispersions of micelles in PBS did not lead to a further decrease in particle size. Based on these results, we can expect that dimensions of ALN-m/DTX under physiological conditions will be around 60 nm and thus will be suitable for bone targeting and extravasation since the pore size of the capillaries and sinusoids in the bone marrow is approximately 80–100 nm[31]. Dispersions of DTX-loaded micelles exhibited good stability as no changes in size or PDI were detected within at least 4 weeks of storage at ambient conditions.

Both DTX-loaded formulations displayed similar sustained release profiles without burst release (Figure 1A). Under physiological conditions (PBS, pH 7.4) the cumulative release of DTX from both types of micelles was about 25% within 12 h. The slightly slower release rates were observed for ALN-m/DTX as compared to ALK-m/DTX at longer periods of times. DTX release from ALN-m/DTX was further slowdown in the presence of serum albumin in the medium (70% FBS). These data suggest that limited drug leakage from the micelles can be expected in the circulation, which is the first step of the successful delivery.

Bone mineral binding of ALN-decorated micelles.

The bone targeting and retention capacity of ALN-m/DTX were evaluated using HA powder as a bone mineral mimicking model[32]. To this end, we have screened a series of fluorescently-labeled ALN-decorated micelles with various content of ALN moieties that was controlled by the molar ratio of fluorescently labeled ALK-PEG-PGlu-PPhA and ALN-

PEG-PGlu-PPhA copolymers. The measurements of HA-associated fluorescence confirmed that all bone-targeted micelles exhibited a good affinity to HA as a result of multivalent interactions and anchoring via ALN moieties (Figure 1B). As expected the binding of targeted ALN-m exceeded that of the non-targeted ALK-m and became more efficient as the density of targeting ligands increased. The bound fraction of ALN-m reached saturation level (approximately 70%) for the ALN-m with 37 mol % ALN moieties on their surfaces and a further increase in ligand density did not provide statistically significant improvements in HA binding. The observed effect of ALN density can be partially attributed to improper ligand presentation since ALN moieties attached to the flexible PEG chains may be buried in the shell surrounding the core of the micelles or steric hindrance of the ligands due to the size of the micelles. Importantly, the presence of calcium ions in the solution and their chelation by ALN-m did not affect the binding of ALN-m to HA (Figure S4). This is in agreement with the previous reports on the increased affinity of ALN-modified nanoparticles for HA compared to calcium ions in solution and the ability of calcium pre-incubated nanoparticles to adsorb on HA surfaces[33]. In view of these observations, it is likely that ALN-m could retain their ability to bind to the bone mineral matrix in the presence of calcium ions in the bloodstream upon intravenous administration. In addition, since calcium-bound ALN-m had less negative ζ-potential (Table 1), this observation also supports the argument that binding of ALN-m to HA is mainly driven by specific interactions via ALN moieties rather than by the negative ζ-potential of the micelles. In this context, it is also noteworthy that non-targeted ALK-m displayed relatively high binding efficiency (ca. 20%, Figure 1B). It may be attributed to the contribution of binding via PGlu block in the outer shell of the micelles. Indeed, it is well known that aspartic acid or glutamic acid oligopeptides have an affinity for HA. Their binding capacity increases when repeating sequences of amino acid residues are present in the sequence such as in osteopontin and sialoprotein, non-collagenous bone proteins[34]. Thus, it is likely that incorporation of short hydrophilic PGlu blocks (10 units) into the shell of the ALN-m may be beneficial not only for stabilization of micellar structures but also by enabling additional binding capabilities. Overall, these data suggest that ALN-m could be a suitable drug carrier to target chemotherapeutics to the bone resorption sites. Besides being an excellent bone targeting agent, ALN pharmacological mechanism of action also involves an inhibitory effect on osteoclasts as well as beneficial effects on osteocytes and osteoblasts[32]. It was also suggested that in addition to anti-resorptive properties bisphosphonates may also have indirect effects on tumor cells[35]. To evaluate whether the design of our delivery system can capitalize on the above-mentioned ALN properties, we choose ALN-m with maximal content of conjugated ALN moieties (ca. 75 mol %) for further experiments.

In vitro cytotoxicity studies.

Murine 4T1 triple-negative breast cancer cell line is known to be highly invasive, relatively resistant to chemotherapy and radiotherapy[36] and is widely used to establish primary or metastatic tumor models in Balb/C mice. The cytotoxic effect of DTX loaded into the polymeric micelles was first evaluated against 4T1 cells using MTT assay. As summarized in Table 2, cytotoxicity of the DTX formulated into ALN-m (referred to as ALN-m/DTX) was substantially increased compared to ALK-m/DTX or conventional DTX formulation (Tween 80/ethanol/PEG300): the IC_{50} value for ALN-m/DTX was 0.035 ± 0.016 μM, an

order of magnitude lower than those for other treatments. Interestingly, when the micelle formulations were tested under the conditions mimicking hypercalcemia (3.4 mM Ca^{2+}), the IC_{50} values were further lowered. Of note, both ALN-m and ALK-m were nontoxic to 4T1 cells in the whole range of concentrations used for the treatment with DTX-loaded formulations (Figure S5). To further validate these results, an additional study was conducted using a clonogenic assay (Figure 1C). Reduction in the colony-forming potential of 4T1 cells was observed following a 36 h exposure to all DTX formats. Consistent with MTT assay results, ALN-m/DTX showed the most potent cytotoxicity and resulted in significantly lower ($p < 0.05$) fraction of surviving cells. The different cytotoxicity profiles of ALN-modified and non-modified DTX-loaded micelles might be ascribed to the enhanced cellular association of ALN-m/DTX by the 4T1 cell. Indeed, it was found that the intracellular accumulation of ALN-m/DTX exceeded that of ALK-m/DTX (Figure S6).

Remodeling of the tumor-bone microenvironment.

As a therapeutic agent ALN was reported to inhibit osteoclast formation and limit their resorptive activity. ALN was also reported to indirectly affect osteoclast precursors, a source of resorption-stimulating cytokines[37]. We next investigated whether ALN moieties tethered to the surface of the micelles could retain its inhibitory effect on osteoclast formation *in vitro*. Murine monocyte/macrophage-like RAW264.7 cells that maintain the capacity to differentiate into osteoclast-like cells in the presence of RANKL were used in these studies. To this end, osteoclast precursor RAW264.7 cells were stimulated by RANKL (50 ng/mL) with or without free ALN or ALN-m in the culture medium. Generation of RAW-derived osteoclasts were confirmed by staining of TRAP enzyme, a marker for osteoclasts. As shown in Figure 2A, treatment with ALN-m attenuated osteoclasts formation in a concentration-dependent manner similarly to free ALN. The IC50 values for free ALN and ALN-m (6.4 ± 2.5 μM and 8.8 ± 4.6 μM, respectively) did not vary significantly from each other ($p > 0.05$). Importantly, treatment with ALK-m did not have any noticeable effect on osteoclastogenesis (Figure 2B). The tumor cells are also known to play a critical role in this cycle by cleaving anchored RANKL into soluble format via elevated expression of MMP-7[38]. Thus, we next performed osteoclastogenesis assay using the conditioned medium (CM) from cultured 4T1 cells that contained secreted differentiation factors. Consistent with the former results, ALN-m significantly repressed ($p < 0.01$) the formation of mature RAW-derived osteoclasts at the ALN concentration corresponding to its IC50 value (9 μM) (Figure 2C). In contrast, multiple multinucleated osteoclasts were derived from RAW264.7 cells treated with 4T1-CM containing ALK-m at the same polymer concentration. These results suggest that ALN-m provide substantial inhibitory capacity against cancer-induced osteoclastogenesis.

In breast cancer bone metastasis microenvironment bi-directional interactions between osteoclasts and tumor cells lead to both osteolysis and tumor growth[39]. Hence, it is also crucial to decrease osteoclast resorptive activity. To evaluate the effects of ALN-m on osteoclast bone lytic activity, RAW264.7 cells were seeded on plates coated with microcrystalline calcium phosphate and then stimulated with RANKL in the absence or presence of ALN-m. We selected two concentrations of ALN-m, 9 μM and 0.81 μM (on ALN basis) that were determined to suppress or not affect osteoclast differentiation,

respectively. The resorption activity was quantified as a total resorptive area of “pits” formed by osteoclasts (Figure 3A). As expected, non-targeted ALK-m did not affect their resorption activity while treatment with ALN-m suppressed formation of resorption pits. Treatment with 0.81 μM ALN-m, the concentration that practically did not inhibit osteoclast differentiation, significantly reduced ($p < 0.01$) overall area of resorption pits compared with RANKL-stimulated cells. Osteoclastic bone resorption was inhibited practically completely by the treatment with 9 μM ALN-m which is in line with our observation that ALN-m at this concentration also significantly inhibit osteoclast formation (Figure 2C). To exclude the direct effect of ALN-m on osteoclastogenesis, in parallel experiment RAW264.7 cells were first pre-differentiated into osteoclasts for 4 days and then were treated with ALN-m. As shown in Figure 3B, osteoclasts treatment with ALN-m significantly inhibited their resorption activity in a concentration-independent manner. Together these results implicate that the ALN-m have an inhibitory activity on both osteoclast differentiation and function and thus could provide additional benefit in combating bone metastases by intervening the disease-induced bone loss.

In the osteolytic cycle in bone metastases, residential macrophages and circulating monocytes stimulating by the cytokines secreted by the tumor can be recruited and infiltrated into the tumor microenvironment[40,41]. The tumor-associated macrophages are not only capable of osteoclast differentiation but also are considered to be involved in angiogenesis, immunosuppression and thus contribute to progressive disease and poor chemotherapy response. Here, we aimed to determine whether ALN- m were able to attenuate macrophage recruitment by cancer cells *in vitro*. To this end, we used the Transwell method where the Raw264.7 cells were seeded on the upper insert and allowed to migrate across the membrane to the lower chamber, on which 4T1 cells were seeded (Figure 4A). In the 24 h period, a substantial number of the macrophages were found to migrate across the membrane toward 4T1 cells, with more than a 10-fold increase in a number of migrated cells compared to the negative control (Figure 4, B and C). When treated with ALN-m, as low as 0.81 μM on ALN base, migration ability of macrophages was suppressed to a practically negligible level ($p > 0.05$ compared to negative control). Given that ALN-m at such concentration is non-toxic to both types of cells, it could be assumed that the “cooperation” between tumor and macrophage was inhibited.

In vivo therapeutic efficacy.

Before assessing the therapeutic efficacy of DTX-loaded micelles, we evaluated the pharmacokinetics of both ALN-m/DTX and ALK-m/DTX in healthy Balb/C mice and compared to “free” DTX (in Tween 80/ethanol/PEG300) at an equivalent dose of 10 mg DTX/kg. The non-compartment model PK parameters are presented in Supplementary Table S2. DTX incorporation into micelles resulted in a modest increase in plasma half-life (8.9 h for ALN-m/DTX and 7.7 h for ALK-m/DTX vs. 6.2 h for free DTX). Moreover, DTX plasma exposure as determined by the area-under-the-curve (AUC) was ~1.5 times higher for ALN-m/DTX than that for ALK-m/DTX. Both the volume of distribution and clearance were decreased by 1.3-fold and 1.5-fold, respectively, in the ALN-m/DTX treatment group compared with the ALK-m/DTX treatment group. It is likely that the observed trend may be related to the presence of hydrophilic and negatively charged ALN moieties on the surface

of the micelles that provide additional hydration layer and more favorable nano-biointerface compared to more hydrophobic ALK groups on the surface of ALK-m. While a better understanding of the effects of surface modifications on stealth properties of ALN-m is needed, these preliminary data suggest that ALN-m can prolong circulation time of DTX through reducing its rapid elimination and contributing to more DTX distributed into bone tissue.

Syngeneic 4T1 breast cancer model was used to assess the therapeutic effect of ALN-m/DTX on established bone metastases[42]. To establish disseminated metastatic disease, 4T1/Luc cells were injected into a left cardiac ventricle of Balb/C mice. Bone metastatic seeding and burden was monitored by whole body BLI. The disease was found to be very aggressive and associated with substantial weight loss: tumor burden exclusively inside the skeleton was successfully established in 1–2 weeks after cell injection and often resulted in mortality within 3 weeks. Due to the aggressiveness of the disease, the treatments were administered daily for the first three days to assure that all individual experimental subjects received the same total dose of the drug. In this model of aggressive bone metastasis, we observed a trend of delayed progression of bone metastasis by treatment with either ALN-m/DTX or ALK-m/DTX compared with the control group ($p < 0.05$, Figure 5A and Figure S6). In addition, both treatments attenuated animal weight loss (the effect of ALN-m/DTX was statistically significant, $p < 0.02$ *vs.* control group) and can also be indicative of their therapeutic potential (Figure 5B). This is in contrast with the treatment of DTX, which had a negligible effect on reducing bone metastasis ($p \approx 0.28$ versus the control group), which can be explained by the aggressiveness of the disease model and the drug-resistant nature of the 4T1 cell line. Of note, neither of the micelles-based formulations reached statistical significance compared to free DTX treatment at the endpoint of the BLI monitoring (18 days) when the mice in the control group succumbed to metastatic cancer. This seems to indicate that frequent administration of the DTX-loaded micelles may cause a continuous drug supply to the tumor sites, where the targeting properties of the carrier become irrelevant. Considering similar size (about 60 nm) of both targeted and non-targeted micelles and only modest improvement in PK parameters of ALN-m/DTX compared to ALK-m/DTX, we would not expect a major difference in the extent of DTX delivery between these two formulations due to EPR effect. The equilibrium of micelle movement in and out of the tumor site might be shifted toward prolonged local residence time of the ALN-m/DTX due to their bone-binding properties.

Moreover, ALN-m could provide additional benefit in combating bone metastases by reducing osteoclast activity and support of tumor growth by tumor-associated macrophages. Therefore, it is fair to presume that the direct and indirect effects of ALN-m/DTX would have benefited over ALK-m/DTX or DTX alone in the long-term. Indeed, the treatment with free DTX did not provide any improvement in animal survival over the saline control (Figure 5C). The non-targeted ALK-m/DTX slightly prolonged the mean survival time from 18 to 21 days, although all mice reached the endpoint before day 24. Remarkably, the ALN-m/DTX demonstrated the best therapeutic outcome and significantly improved the survival time ($p < 0.05$) compared to ALK-m/DTX group with 2 out of 5 long-term survivors who reached the endpoint at day 35 (Figure 5C). Such a therapeutic response to ALN-m/DTX is far superior to either ALK-m/DTX or DTX alone suggesting a benefit of bone targeting and

chemotherapy in late-stage bone metastasis. Notably, no visceral organ toxicities were observed as a result of the treatments as representatively assessed for liver, spleen and kidney by tissue histopathology analysis (Figure S8). Extramedullary hematopoiesis is often reported as a consequence of bone metastases in this model[43]. In the control group, strong extramedullary hematopoiesis was detected in the liver, while in the treatment groups it was significantly reduced. Marrow toxicity indicated by decreased cellularity was occasionally present in the bone sections, but was similar between groups. These observations suggest a favorable toxicity profile for the DTX micellar formulations.

Among all treatment options for metastatic breast cancer including chemotherapy, hormonal therapy and targeted therapy, radiation therapy (RT) remains an essential modality particularly for the palliative purpose. The most common utilities of palliative RT are for pain control, improving ambulation, preventing fractures and controlling spinal cord compression/neurologic deficits and preserving the quality of life particularly for patients with bone metastasis. Over the past few decades, multiple randomized controlled clinical trials have confirmed equivalent short-term pain relief between a single 8 Gray (Gy) fraction and multiple fraction regimens, including most commonly 30 Gy in 10 fractions, 24 Gy in 6 fractions and 20 Gy in 5 fractions[44–48]. While single fraction treatment optimized convenience of patients and their caregivers and was linked to lower acute toxicity, retreatment rates due to recurrent pain at the same anatomic site were higher in those patients who received single fractions compared to fractionated treatment courses. It is important for further studies to explore the possibilities of combined therapy to enhance the efficacy of single fraction RT. To test this notion, we conducted a proof-of-concept experiment utilizing sequential chemotherapy with ALN-m/DTX and RT. Two groups of animals with developed metastasis received three i.v. injections daily of either saline or ALN-m/DTX (10 mg/kg on DTX basis) and then, 24 h after the last treatment, mice received a total of 5 Gy of radiation at a dose rate of 3 Gy/min. The treatment of late-stage metastasis with a single 5 Gy RT was ineffective and did not delay the progression of the disease (Figure 6A). In contrast, the administration of ALN-m/DTX followed by RT delayed tumor growth and prolonged the median survival from 19 days (RT) to 30 days (Figure 6B). Due to the large variations within the RT group (Figure S7), the differences in tumor growth or survival between RT and combination group was close to but not statistically significant ($p = 0.06$ *vs.* the RT-only treatment group). Further detailed studies are needed to confirm the benefits of this combined treatment regimen. Particularly, it might be interesting to test this combination therapy in another model of bone metastasis, when breast cancer cells are injected directly into bone (such as tibia or femur). While it is technically not a model of metastasis, it can replicate tumor-induced changes in bone[42] and will permit to apply RT locally. Nevertheless, these results suggest that treatment with bone-targeted chemotherapy combined with radiotherapy could potentially be more effective and suppress the development and dissemination of bone metastasis.

CONCLUSIONS

We engineered a dual-functional bone-homing drug carrier based on biodegradable polypeptide-based micelles that can deliver the drug to the bone and shows a propensity for simultaneous remodeling the tumor-bone microenvironment. The drug-loaded micelles were

prepared via a robust procedure that allowed higher loading of docetaxel using an alendronate-modified copolymer with a relatively short length of the hydrophobic segment. Docetaxel, when encapsulated into the ALN-m was found to retain its cytotoxicity and to be even more effective in 4T1 breast cancer cell killing in the conditions mimicking hypercalcemia in patients with metastases. These ALN-m demonstrated enhanced binding to the bone mineral analog and were effective in inhibiting osteoclast differentiation and their resorption activity as well as attenuate tumor-induced migration of macrophages *in vitro*. In line with the *in vitro* results, ALN-m/DTX delayed disease progression and improved survival in a syngeneic murine model of breast cancer bone metastasis. This model represents a useful tool for examining the later stages of breast cancer bone metastasis, however, the skeletal sites of metastatic deposition and number and size of the metastases are extremely variable. Nevertheless, our work provides new insight into the fusion of ALN moieties with drug-loaded micelles to maximize the therapeutic efficiency of chemotherapy by targeting bone metastases and their microenvironment.

Supplementary Material

Refer to Web version on PubMed Central for supplementary material.

ACKNOWLEDGMENTS

This work was supported by a Cancer Nanotechnology Platform Partnership grant (U01 CA198910) of the National Cancer Institute Alliance for Nanotechnology in Cancer (T.B.). We acknowledge the technical supprt of the Nanomaterials Core Facility of the Center for Biomedical Research Excellence (CoBRE), Nebraska Center for Nanomedicine supported by the Institutional Development Award from the National Institute of General Medical Sciences under grant number P30GM127200. T. L. is grateful to the China Scholarship Council (CSC) for a graduate studies fellowship (CSC[2003]3009). We are also grateful to Hong Jun Wang for helping with the development of the metastatic breast cancer model, and to Virender Kumar and Sushil Kumar for providing advice in the PK analysis.

REFERENCES

(1). Chen Y-C; Sosnoski DM; Mastro AM Breast Cancer Metastasis to the Bone: Mechanisms of Bone Loss. Breast Cancer Res 2010, 12 (6), 215. [PubMed: 21176175]

(2). Fang J; Xu Q Differences of Osteoblastic Bone Metastases and Osteolytic Bone Metastases in Clinical Features and Molecular Characteristics. Clin Transl Oncol 2015, 17 (3), 173–179. [PubMed: 25351174]

(3). Cleeland C; Moos von R; Walker MS; Wang Y; Gao J; Chavez-MacGregor M; Liede A; Arellano J; Balakumaran A; Qian Y Burden of Symptoms Associated with Development of Metastatic Bone Disease in Patients with Breast Cancer. Support Care Cancer 2016, 24 (8), 3557–3565. [PubMed: 27022965]

(4). Kingsley LA; Fournier PGJ; Chirgwin JM; Guise TA Molecular Biology of Bone Metastasis. Mol. Cancer Ther 2007, 6 (10), 2609–2617. [PubMed: 17938257]

(5). O'Carrigan B; Wong MH; Willson ML; Stockler MR; Pavlakis N; Goodwin A Bisphosphonates and Other Bone Agents for Breast Cancer. Cochrane Database Syst Rev 2017, 10 (10), CD003474. [PubMed: 29082518]

(6). Kuchuk I; Hutton B; Moretto P; Ng T; Addison CL; Clemons M Incidence, Consequences and Treatment of Bone Metastases in Breast Cancer Patients-Experience From a Single Cancer Centre. J Bone Oncol 2013, 2 (4), 137–144. [PubMed: 26909284]

(7). Wang D; MILLER S; Kopečková P; KOPECEK J Bone-Targeting Macromolecular Therapeutics. Adv. Drug Deliv. Rev 2005, 57 (7), 1049–1076. [PubMed: 15876403]

(8). Cole LE; Vargo-Gogola T; Roeder RK Targeted Delivery to Bone and Mineral Deposits Using Bisphosphonate Ligands. Adv. Drug Deliv. Rev 2016, 99 (Pt A), 12–27. [PubMed: 26482186]

(9). Love C; Din AS; Tomas MB; Kalapparambath TP; Palestro CJ Radionuclide Bone Imaging: an Illustrative Review. Radiographics 2003, 23 (2), 341–358. [PubMed: 12640151]

(10). Ramanlal Chaudhari K; Kumar A; Megraj Khandelwal VK; Ukawala M; Manjappa AS; Mishra AK; Monkkonen J; Ramachandra Murthy RS Bone Metastasis Targeting: a Novel Approach to Reach Bone Using Zoledronate Anchored PLGA Nanoparticle as Carrier System Loaded with Docetaxel. J Control Release 2012, 158 (3), 470–478. [PubMed: 22146683]

(11). Wang X; Yang Y; Jia H; Jia W; Miller S; Bowman B; Feng J; Zhan F Peptide Decoration of Nanovehicles to Achieve Active Targeting and Pathology-Responsive Cellular Uptake for Bone Metastasis Chemotherapy. Biomater Sci 2014, 2 (7), 961–971. [PubMed: 26082834]

(12). Thamake SI; Raut SL; Gryczynski Z; Ranjan AP; Vishwanatha JK Alendronate Coated Poly-Lactic-Co-Glycolic Acid (PLGA) Nanoparticles for Active Targeting of Metastatic Breast Cancer. Biomaterials 2012, 33 (29), 7164–7173. [PubMed: 22795543]

(13). Fernandes C; Monteiro S; Belchior A; Marques F; Gano L; Correia JDG; Santos I Novel (188)Re Multi-Functional Bone-Seeking Compounds: Synthesis, Biological and Radiotoxic Effects in Metastatic Breast Cancer Cells. Nucl. Med. Biol 2016, 43 (2), 150–157. [PubMed: 26872439]

(14). Ye W-L; Zhao Y-P; Li H-Q; Na R; Li F; Mei Q-B; Zhao M-G; Zhou S-Y Doxorubicin-Poly (Ethylene Glycol)-Alendronate Self-Assembled Micelles for Targeted Therapy of Bone Metastatic Cancer. Sci Rep 2015, 5 (1), 14614. [PubMed: 26419507]

(15). Miller K; Eldar-Boock A; Polyak D; Segal E; Benayoun L; Shaked Y; Satchi-Fainaro R Antiangiogenic Antitumor Activity of HPMA Copolymer-Paclitaxel-Alendronate Conjugate on Breast Cancer Bone Metastasis Mouse Model. Molecular Pharmaceutics 2011, 8 (4), 1052–1062. [PubMed: 21545170]

(16). Clementi C; Miller K; Mero A; Satchi-Fainaro R; Pasut G Dendritic Poly(Ethylene Glycol) Bearing Paclitaxel and Alendronate for Targeting Bone Neoplasms. Molecular Pharmaceutics 2011, 8 (4), 1063–1072. [PubMed: 21608527]

(17). Miller K; Clementi C; Polyak D; Eldar-Boock A; Benayoun L; Barshack I; Shaked Y; Pasut G; Satchi-Fainaro R Poly(Ethylene Glycol)-Paclitaxel-Alendronate Self-Assembled Micelles for the Targeted Treatment of Breast Cancer Bone Metastases. Biomaterials 2013, 34 (15), 3795–3806. [PubMed: 23434349]

(18). Desale SS; Cohen SM; Zhao Y; Kabanov AV; Bronich TK Biodegradable Hybrid Polymer Micelles for Combination Drug Therapy in Ovarian Cancer. J Control Release 2013, 171 (3), 339–348. [PubMed: 23665258]

(19). Srinivasan R; Tan LP; Wu H; Yang P-Y; Kalesh KA; Yao SQ High-Throughput Synthesis of Azide Libraries Suitable for Direct “Click” Chemistry and in Situ Screening. Org. Biomol. Chem 2009, 7 (9), 1821–1828. [PubMed: 19590777]

(20). Ananthapadmanabhan KP; Goddard ED; Turro NJ; Kuo PL Fluorescence Probes for Critical Micelle Concentration. Langmuir 1985, 1 (3), 352–355. [PubMed: 21370917]

(21). Zhang S; Wright JEI; Bansal G; Cho P; Uludag H Cleavage of Disulfide-Linked Fetuin-Bisphosphonate Conjugates with Three Physiological Thiols. Biomacromolecules 2005, 6 (5), 2800–2808. [PubMed: 16153121]

(22). Ferrari M; Fornasiero MC; Isetta AM MTT Colorimetric Assay for Testing Macrophage Cytotoxic Activity *in Vitro*. Journal of Immunological Methods 1990, 131 (2), 165–172. [PubMed: 2391427]

(23). Lelekakis M; Moseley JM; Martin TJ; Hards D; Williams E; Ho P; Lowen D; Javni J; Miller FR; Slavin J A Novel Orthotopic Model of Breast Cancer Metastasis to Bone. Clinical & experimental metastasis 1999, 17 (2), 163–170. [PubMed: 10411109]

(24). Yasugi K; Nagasaki Y; Kato M: Kataoka K Preparation and characterization of polymer micelles from poly(ethylene glycol)-poly(D,L-lactide) block copolymers as potential drug carrier. J Control Release 1999, 62 (1–2), 89–100. [PubMed: 10518640]

(25). Pierri E; Avgoustakis K Poly(Lactide)-Poly(Ethylene Glycol) Micelles as a Carrier for Griseofulvin. J Biomed Mater Res A 2005, 75 (3), 639–647. [PubMed: 16110497]

(26). Logie J; McLaughlin CK; Tam RY; Shoichet MS Innovative Use of the Taxol Binding Peptide Overcomes Key Challenges of Stable and High Drug Loading in Polymeric Nanomicelles. Chem. Commun 2015, 51 (60), 12000–12003.

(27). Lyseng-Williamson KA; Fenton C Docetaxel: a Review of Its Use in Metastatic Breast Cancer. Drugs 2005, 65 (17), 2513–2531. [PubMed: 16296875]

(28). Jones SE; Erban J; Overmoyer B; Budd GT; Hutchins L; Lower E; Laufman L; Sundaram S; Urba WJ; Pritchard KI; Mennel R; Richards D; Olsen S; Meyers ML; Ravdin PM Randomized Phase III Study of Docetaxel Compared with Paclitaxel in Metastatic Breast Cancer. J. Clin. Oncol 2005, 23 (24), 5542–5551. [PubMed: 16110015]

(29). Schwartzberg LS; Navari RM Safety of Polysorbate 80 in the Oncology Setting. Adv Ther 2018, 35 (6), 754–767. [PubMed: 29796927]

(30). Rosner MH; Dalkin AC Onco-Nephrology: the Pathophysiology and Treatment of Malignancy-Associated Hypercalcemia. Clinical Journal of the American Society of Nephrology 2012, 7 (10), 1722–1729. [PubMed: 22879438]

(31). Tye CE; Rattray KR; Warner KJ; Gordon JAR; Sodek J; Hunter GK; Goldberg HA Delineation of the Hydroxyapatite-Nucleating Domains of Bone Sialoprotein. J. Biol. Chem 2003, 278 (10), 7949–7955. [PubMed: 12493752]

(32). Russell RGG; Watts NB; Ebetino FH; Rogers MJ Mechanisms of Action of Bisphosphonates: Similarities and Differences and Their Potential Influence on Clinical Efficacy. Osteoporos Int 2008, 19 (6), 733–759. [PubMed: 18214569]

(33). Laura De Miguel MN; Georgiana Surpateanu; Bogdan I Iorga; Gilles Ponchel. Poly(γ-benzyl-l-glutamate)-PEG-alendronate multivalent nanoparticles for bone targeting. International Journal of Pharmaceutics 2014, 460, 73–82. [PubMed: 24211357]

(34). Tavafoghi M; Cerruti M The Role of Amino Acids in Hydroxyapatite Mineralization. J R Soc Interface 2016, 13 (123).

(35). Clézardin P; Ebetino FH; Fournier PGJ Bisphosphonates and Cancer-Induced Bone Disease: Beyond Their Antiresorptive Activity. Cancer Res 2005, 65 (12), 4971–4974. [PubMed: 15958534]

(36). Frings PWH; Van Elssen CHMJ; Wieten L; Matos C; Hupperets PSJG; Schouten HC; Bos GMJ; Van Gelder M Elimination of the Chemotherapy Resistant Subpopulation of 4T1 Mouse Breast Cancer by Haploidentical NK Cells Cures the Vast Majority of Mice. Breast Cancer Res. Treat 2011, 130 (3), 773–781. [PubMed: 21274621]

(37). D'Amelio P; Grimaldi A; Cristofaro MA; Ravazzoli M; Molinatti PA; Pescarmona GP; Isaia GC Alendronate Reduces Osteoclast Precursors in Osteoporosis. Osteoporos Int 2010, 21 (10), 1741–1750. [PubMed: 19949772]

(38). Lynch CC; Hikosaka A; Acuff HB; Martin MD; Kawai N; Singh RK; Vargo-Gogola TC; Begtrup JL; Peterson TE; Fingleton B; Shirai T; Matrisian LM; Futakuchi M MMP-7 Promotes Prostate Cancer-Induced Osteolysis via the Solubilization of RANKL. Cancer Cell 2005, 7 (5), 485–496. [PubMed: 15894268]

(39). Mundy GR Metastasis to Bone: Causes, Consequences and Therapeutic Opportunities. Nature Reviews Cancer 2002, 2 (8), 584–593. [PubMed: 12154351]

(40). Vasiliadou I; Holen I The Role of Macrophages in Bone Metastasis. J Bone Oncol 2013, 2 (4), 158–166. [PubMed: 26909287]

(41). Sousa S; Määttä J The Role of Tumour-Associated Macrophages in Bone Metastasis. J Bone Oncol 2016, 5 (3), 135–138. [PubMed: 27761375]

(42). Simmons JK; Hildreth BE; Supsavhad W; Elshafae SM; Hassan BB; Dirksen WP; Toribio RE; Rosol TJ Animal Models of Bone Metastasis. Vet. Pathol 2015, 52 (5), 827–841. [PubMed: 26021553]

(43). Johns JL; Christopher MM Extramedullary Hematopoiesis: a New Look at the Underlying Stem Cell Niche, Theories of Development, and Occurrence in Animals. Vet. Pathol 2012, 49 (3), 508–523. [PubMed: 22262354]

(44). Gaze MN; Kelly CG; Kerr GR; Cull A; Cowie VJ; Gregor A; Howard GCW; Rodger A Pain Relief and Quality of Life Following Radiotherapy for Bone Metastases: a Randomised Trial of

Two Fractionation Schedules. Radiotherapy and Oncology 1997, 45 (2), 109–116. [PubMed: 9423999]

(45). Nielsen OS; Bentzen SM; Sandberg E; Gadeberg CC; Timothy AR Randomized Trial of Single Dose Versus Fractionated Palliative Radiotherapy of Bone Metastases. Radiotherapy and Oncology 1998, 47 (3), 233–240. [PubMed: 9681885]

(46). Steenland E; Leer J; van Houwelingen H; Post WJ; van den Hout WB; Kievit J; de Haes H; Martijn H; Oei B; Vonk E; van der Steen-Banasik E; Wiggenraad RGJ; Hoogenhout J; Wárlám-Rodenhuis C; van Tienhoven G; Wanders R; Pomp J; van Reijn M; van Mierlo T; Rutten E The Effect of a Single Fraction Compared to Multiple Fractions on Painful Bone Metastases: a Global Analysis of the Dutch Bone Metastasis Study. Radiotherapy and Oncology 1999, 52 (2), 101–109. [PubMed: 10577695]

(47). Foro Arnalot P; Fontanals AV; Galcerán JC; Lynd F; Latiesas XS; de Dios NR; Castillejo AR; Bassols ML; Galán JL; Conejo IM; López MA Randomized Clinical Trial with Two Palliative Radiotherapy Regimens in Painful Bone Metastases: 30 Gy in 10 Fractions Compared with 8 Gy in Single Fraction. Radiotherapy and Oncology 2008, 89 (2), 150–155. [PubMed: 18556080]

(48). Hartsell WF; Scott CB; Bruner DW; Scarantino CW; Ivker RA; Roach M; Suh JH; Demas WF; Movsas B; Petersen IA; Konski AA; Cleeland CS; Janjan NA; DeSilvio M Randomized Trial of Short- Versus Long-Course Radiotherapy for Palliation of Painful Bone Metastases. J. Natl. Cancer Inst 2005, 97 (11), 798–804. [PubMed: 15928300]

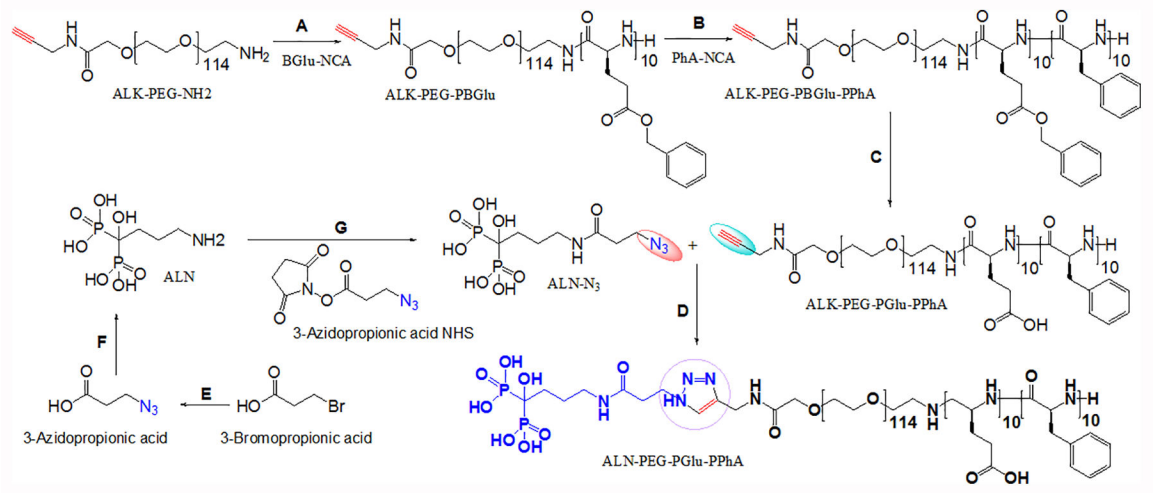

Scheme 1.

Synthesis of the bone-targeted copolymer.

Conditions: A). DMF, 40 °C, N_2, 72 h; B). DMF / 1,4-dioxane, 40 °C, N_2, 120 h; C). THF / 0.5N NaOH, RT, 24 h; D). MeOH / H_2O (1:1, v/v), $CuSO_4 \times 5H_2O$, THPTA, ascorbic acid, Ar, RT; E). ACN, NaN_3, reflux, 6 h; (F) DCM, EDC/NHS, RT, 6 h; (G) ACN/H_2O (1:4, v/v), pH 8.0, RT, 24 h. Abbreviations: Alk-PEG-NH_2 - α-Amino-ω-ALK-poly(ethylene glycol), BGlu-NCA - L-glutamic acid γ-benzyl ester-N- carboxyanhydride, PhA-NCA - L-phenylalanine -N- carboxyanhydride, ALK-PEG-PBGlu-PPhA – alkyne-poly(ethylene glycol)-b-poly(L-glutamic acid γ-benzyl ester)-b-poly(L-phenylalanine), ALK-PEG-PGlu-PPhA – alkyne-poly(ethylene glycol)-b-poly(L-glutamic acid)-b-poly(L-phenylalanine).

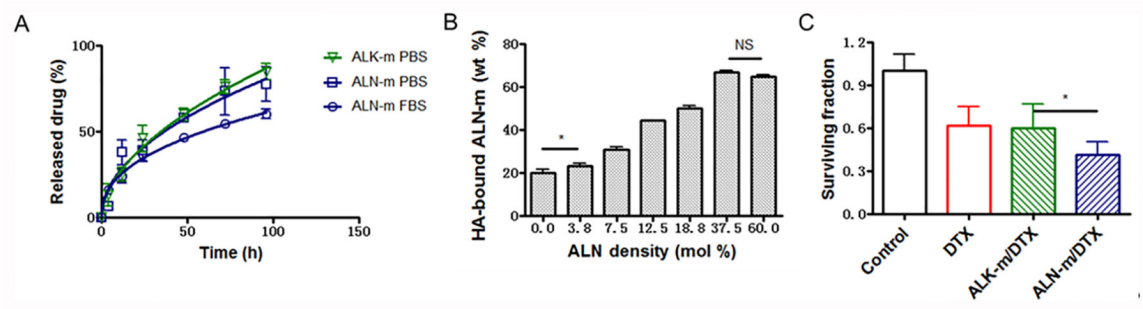

Figure 1. ***In vitro*** **characterization of ALN-m and ALN-m/DTX micelles.**

(A) Drug release profiles for DTX in targeted ALN-m/DTX and non-targeted ALK-m/DTX micelles under physiological conditions as determined by HPLC method; (B) Binding of the ALN-m to the bone mineral HA as a function of degree of modification of ALN-m; (C) Cytotoxicity of DTX and micelle formulations in 4T1 breast cancer cells determined by clonogenic assay. Cells were treated with 0.1 μg/mL DTX equivalents for 36 h and allowed to recover in fresh medium for another 72 h. Data are expressed as mean ± SD (n = 3), *$p < 0.05$, NS - not significant.

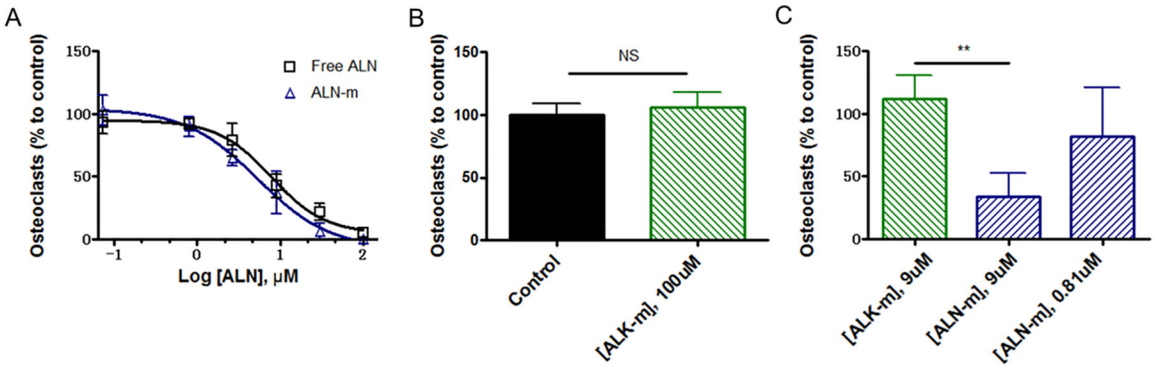

Figure 2. Effects of ALN-m on osteoclastogenesis.

RAW264.7 cells were stimulated with RANKL (50 μg/mL) in the presence or absence of ALK-m or ALN-m at different concentrations (based on ALN equivalents). Mature multinucleated osteoclast cells were detected by TRAP staining. The results are normalized to cells grown only in the presence of RANKL (control). (A) free ALN and ALN-m displayed comparable inhibition effects on osteoclasts differentiation; (B) ALK-m did not show any effect on the osteoclast differentiation; (C) RAW264.7 cells were stimulated with CM from 4T1 cells in the presence or absence of ALN-m. Data presented as the mean ± SD (n = 3). **p < 0.01, NS - not significant.

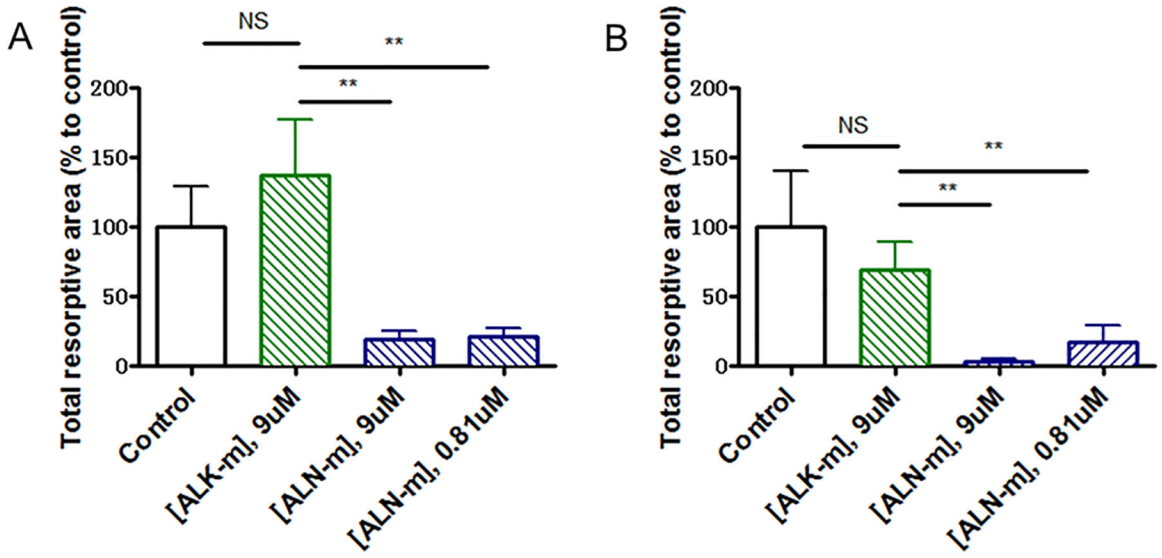

Figure 3. ALN-m inhibits the resorption activity of osteoclasts.

(A) RAW264.7 cells were cultured on Osteo Surface plates and treated with RANKL (50 μg/mL) in the presence or absence of ALK or ALN-m as indicated. Polymer concentration is expressed based on ALN equivalents. The total area of the resorbed regions was quantified and normalized to the cells cultured in the presence of only RANKL (control). (B) RAW264.7 cells were first differentiated into osteoclasts on Osteo Surface plates in the presence of RANKL (50 μg/mL) for 4 days and then treated with ALK-m or ALN-m for next 3 days. Data are expressed as the mean ± SD (n = 3). **p < 0.01, NS - not significant.

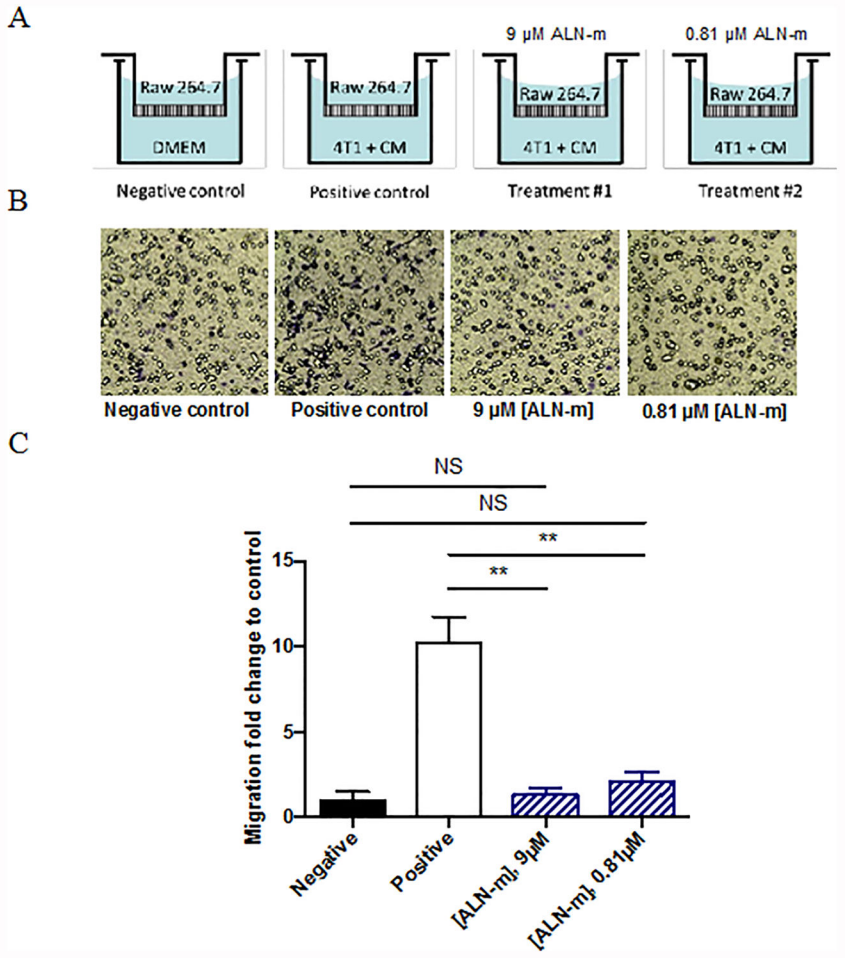

Figure 4. Inhibition of tumor-induced macrophage migration by ALN-m.

(A) Schematic illustration of the experiment. RAW264.7 cells (10^3 per insert) were added to the upper chamber with DMEM without FBS (negative control) or 4T1 cells (10^5/well) and their conditioned media (CM) added to the lower well (positive control). RAW264.7 cells were allowed to migrate for 24 h at 37°C prior to staining and quantitation of chemotaxis. In experimental groups ALN-m were added to both chambers; (B) Representative images of migrated RAW264.7 cells; (C) Quantification of migration of RAW264.7 cells treated with ALN-m. Data represents the average ±SD for 5 randomly selected fields over 3 separate experiments. **$p < 0.01$, NS - not significant.

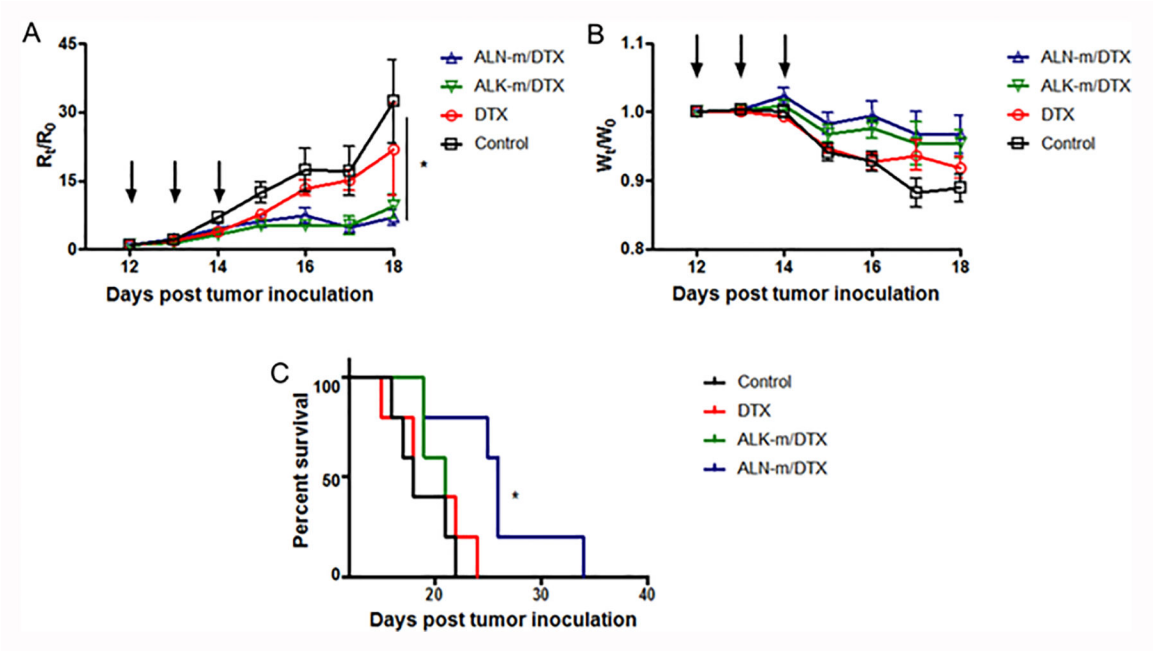

Figure 5. Anti-metastatic efficacy of ALN-m/DTX in syngeneic 4T1 breast cancer bone metastasis model.

Treatment consisted of iv injections of PBS, DTX (in Tween 80/ethanol/PEG300), ALK-m/DTX, or ALN-m/DTX at an equivalent dose of 10 mg DTX/kg. Arrows represent iv injections. (A) Quantification of bone metastasis burden based on whole body BLI imaging; (B) Body weight; (C) Kaplan−Meier survival plot; (D) Histopathological analysis of representative kidney, liver, and spleen of mice received different treatments. Data presented as mean ± SEM (n = 8). *p < 0.05 by log-rank (Mantel-Cox) test.

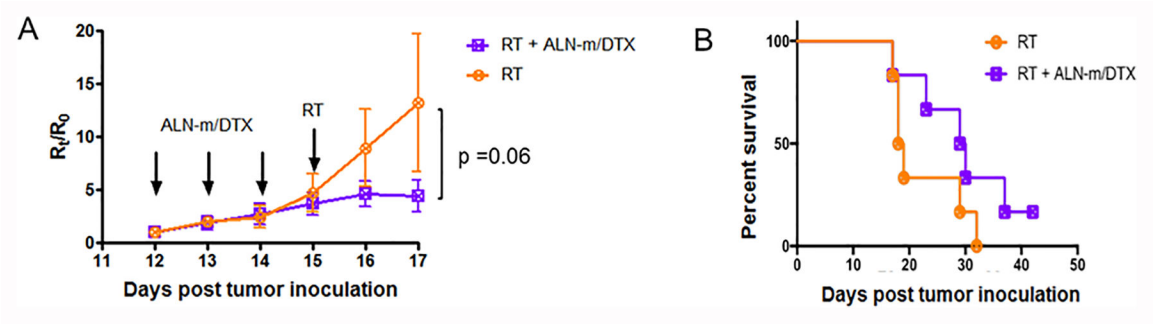

Figure 6. Treatment efficiencies of sequential chemotherapy with ALN-m/DTX and radiotherapy (RT).

Treatment consisted of iv injections of PBS or ALN-m/DTX (10 mg/kg DTX) followed by 5 Gy of radiation at a dose rate of 3 Gy/min 24 h after the last injection. Arrows represent iv injections. (A) Quantification of bone metastasis burden based on whole body BLI imaging; (B) Kaplan−Meier survival plot. Data presented as mean ± SEM (n = 6).

Table 1.

Physicochemical characteristics of DTX-loaded micelles

Sample	DI water				DI water with 3.4 mM Ca^{2+}			PBS	
	D_{eff}[a] (nm)	PDI[a]	ζ-potential[a] (mV)	LC (%)	D_{eff} (nm)	PDI	ζ-potential (mV)	D_{eff} (nm)	PDI
ALK-m/DTX	82 ± 4	0.20	−17 ± 1	22.4	73 ± 1	0.17	−6 ± 1	60	0.16
ALN-m/DTX[b]	84 ± 5	0.18	−30 ± 2	22.4	57 ± 1	0.16	−12 ± 1	67 ± 2	0.16

[a] Effective diameter (D_{eff}), polydispersity index (PDI) and ζ-potential were determined by DLS (copolymer concentration 1 mg/mL; 25°C). Data presented as mean ± SD (n = 3).

[b] ALN-m/DTX corresponds to DTX-loaded micelles prepared from ALN-PEG-PGlu-PPhA copolymers.

Table 2.

IC_{50} values of free DTX and DTX-loaded micelles in 4T1 breast cancer cell line.

Sample	IC_{50}, μM[a]	
	RPMI	RPMI (3.4 mM Ca^{2+})
DTX	2.16 ± 0.82	-
ALK-m/DTX	1.39 ± 0.49	0.26 ± 0.05
ALN-m/DTX	0.035 ± 0.002	0.012 ± 0.020

[a]The IC_{50} values expressed as means ± SD (n = 3).